Magnetotransport properties, electronic structure, and microstructure of $La_{0.7}Sn_{0.3}MnO_3$ thin films

T. Y. Cheng,[1,*] C. W. Lin,[2] L. Chang,[2] C. H. Hsu,[3] J. M. Lee,[3] J. M. Chen,[3] J.-Y. Lin,[4] K. H. Wu,[1] T. M. Uen,[1] Y. S. Gou,[1] and J. Y. Juang[1]

[1]*Department of Electrophysics, National Chiao Tung University, Hsinchu 30050, Taiwan*

[2]*Department of Materials Science and Engineering, National Chiao Tung University, Hsinchu 30050, Taiwan*

[3]*National Synchrotron Radiation Research Center, Hsinchu 30076, Taiwan*

[4]*Institute of Physics, National Chiao Tung University, Hsinchu 30050, Taiwan*

(Received 27 February 2006; revised manuscript received 25 August 2006; published 30 October 2006)

Single-phase $La_{0.7}Sn_{0.3}MnO_3$ (LSnMO) thin films were fabricated on $LaAlO_3$ (LAO) substrates by pulsed laser deposition (PLD). The as-deposited films, though showed insulating characteristics with no sign of insulator-metal transition (IMT) down to very low temperatures, did display a paramagnetic-ferromagnetic transition (PFT) around 180 K. The x-ray absorption spectroscopy (XAS) of the as-deposited LSnMO films shows signature of Mn^{3+}/Mn^{2+} mixed valence indicating that tetravalent Sn ions may have resulted in electron doping into the e_g band of Mn. The transmission electron microscopy (TEM) analyses on the as-deposited LSnMO films further confirmed that the films are epitaxial with uniform composition distributions. It is suggestive that the doping level of $x=0.3$ in $La_{1-x}Sn_xMnO_3$ can be achieved without disrupting the perovskite structure or any composition inhomogeneity. On the other hand, *ex situ* annealing in oxygen as well as in argon atmosphere, though both drive the films to display IMT and a marked enhancement in the transition temperature, the preservation of LSnMO phase is somewhat doubtful. In the oxygen-annealing case, the evidence from the XAS measurements on Sn ions though showed the existence of tetravalent characteristics, the Hall measurements indicated that the obtained LSnMO films are *p* type in nature. Furthermore, the TEM analyses also revealed the emergence of the Sn compounds, which may ultimately drive the obtained films into La-deficient $La_{1-x}MnO_3$ phases.

DOI: 10.1103/PhysRevB.74.134428 PACS number(s): 75.70.Ak, 75.50.Lk, 81.40.Rs

I. INTRODUCTION

The perovskite manganites, being a representative family of strong-correlated electron system, have been subject of extensive researches.[1,2] In particular, in various hole-doped manganites, the colossal magnetoresistance (CMR) effect, manifested by a paramagnetic-ferromagnetic transition at the Curie temperature (T_c) accompanied by a dramatic decrease in resistivity around a similar temperature (T_{IM}), has been ubiquitously observed and attributed to the charge-spin interaction of mixed-valence Mn^{3+}/Mn^{4+} ions via Zener's seminal double-exchange (DE) mechanism.[3] However, it has been pointed out that DE alone might be inadequate to explain the observed CMR effect in $La_{1-x}Sr_xMnO_3$ and the incorporation of polaron effect induced by electron-phonon interactions arising from the Jahn-Teller splitting of the Mn *d* levels could be essential.[4] On the other hand, despite the extensive success in obtaining the hole-doped manganites over wide range of compositions, efforts in trying to substitute La ion with tetravalent ions and hence make the manganites electron doped have been rather inconclusive. Joseph Joly *et al.*[5] argued that, due to the ion size constraints, it is almost impossible to replace the trivalent La^{3+} ion by tetravalent ions in polycrystalline manganite bulks prepared by solid state reaction. Indeed, early attempts of preparing Ce-doped $RMnO_3$ (R=La,Pr,Nd) manganites by Das and Mandal[6] all showed signatures of mixed phases and hence blurred the interpretation of the obtained results. In particular, the replacement of tetravalent ions to La^{3+} often led to the self-doped $La_{1-x}MnO_{3-\delta}$ with localized multiphase compounds, which might give rise to very similar magnetotransport properties to those of the hole-doped manganites and jeopardize the genuine electron-doped characteristics.[7,8]

Recently, single-phase tetravalent-ion-doped $La_{0.7}Ce_{0.3}MnO_3$ (LCeMO) thin films were successfully fabricated by pulsed laser deposition (PLD).[9–12] It appeared that ionic constraints and stoichiometry conservation could be compromised provided proper growth conditions were chosen. On the other hand, Kawai *et al.*[13] showed that, in their preparation scheme, while the as-grown LCeMO films all displayed ferromagnetic-insulator behavior, the typical metal-insulator transition are recovered only after post annealed under the atmosphere of oxygen and/or argon. The existence of the nanoclustering cerium oxides within the films revealed by the transmission electron microscopy (TEM) analyses has led the authors to conclude that cation deficiencies are responsible for the emergence of the ferromagnetic-metal characteristics, albeit the phase regions identified appeared to be rather minor. On the other hand, Zhang *et al.*[14] reported that the x-ray photoemission spectroscopy (XPS) of the $La_{0.9}Te_{0.1}MnO_3$ prepared by PLD and followed by annealing in the flowing oxygen revealed the signature of 4+ valence states for Te ions. They regarded it as the evidence of electron-doping for the $La_{0.9}Te_{0.1}MnO_3$ films. Chen *et al.*[15] reported that the as-prepared $La_{1-x}Pr_xMnO_3$ (LPMO) bulks with different compositions do not show discernable metal-insulator transition behavior. However, the metal-insulator transition and associated CMR effect were obtained after annealing the samples in argon flow atmosphere. The XPS results of the Pr ions in their

samples featured the characteristics of Pr^{3+} and Pr^{4+} mixture, indicating that the LPMO ceramic might be an electron-doped CMR compound. Compared to the potentially electron-doped CMR materials mentioned above, obtaining single-phase $La_xSn_{1-x}MnO_3$ (LSnMO) represents an even more severe challenge because of an even larger ionic size difference between La^{3+} and Sn^{4+}. Nevertheless, CMR effect has been observed in LSnMO,[16–18] albeit the single-phase samples were hardly obtainable by the solid-state reaction technique and only limited doping ($x=0.1-0.2$) has been achieved in thin film form. Since most manganites display optimum CMR effects around 30% doping and the prominent roles played by lattice degree of freedom in giving rise to both CMR[19] effect and phase-coexistence[20] phenomena, it is desirable to perform systematic studies on the LSnMO system with higher doping. In addition to the experimental facts briefly described above, there are some points noteworthy of mentioning. First, all attempts to substitute the tetravalence ion (Ce, Sn, Te, Pr) into the La ion site frequently result in ferromagnetic-insulator CMR, suggesting either the lack of itinerant carriers or the exchange mechanism may be fundamentally different in the electron-doped regime. Second, post annealing under oxygen or argon environment has been a usual practice in fabricating the electron-doped manganites. However, samples prepared under these two annealing schemes can display markedly different transport and magnetic behaviors. Finally, it is not clear that the electronic states of the doped ions indeed directly reflect the doping states of the CMR materials. In this paper, we present results obtained from the magnetotransport, electronic, and microstructure analyses of the $La_{0.7}Sn_{0.3}MnO_3$ (LSnMO) that evidently clarify some of the outstanding issues mentioned above.

II. EXPERIMTAL

Sintered LSnMO target was prepared by conventional solid-state reaction technique. LSnMO films were deposited on single crystalline $LaAlO_3(100)$ substrates using a 248 nm KrF excimer laser operating at energy density of $2-3$ J/cm^2. The details of the processing conditions can be found elsewhere.[21] The as-deposited films, though displayed usual paramagnetic-ferromagnetic transitions, the typical CMR behaviors of the accompanying insulator-metal transition was, however, absent. Thus, in some cases, subsequent *ex situ* annealing was carried out at 800 °C for 4 h in 250 Torr of oxygen or argon. The temperature dependences of magnetization $[M(T)]$ and magnetotransport properties were measured using a Quantum Design® PPMS system with a maximum applied field strength of 8 Tesla. The crystalline structure of the films was examined by x-ray diffraction (XRD) (θ-2θ scan) and x-ray scattering measurements. For the electronic structure and valence state of Mn and Sn ions, the x-ray absorption near edge spectroscopy (XANES) experiments were performed at the National Synchrotron Radiation Research Center of Taiwan. In order to probe the microstructure, interface between film and substrate, as well as the element distributions of the LSnMO films, cross-section transmission electron microscopy (TEM) and electron energy loss spectroscopy (EELS) mapping were performed.

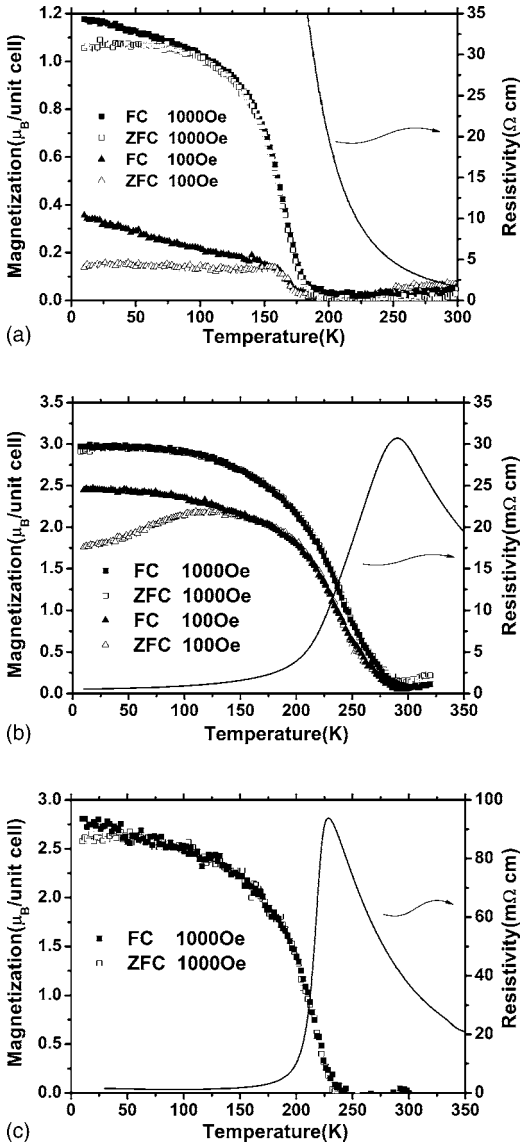

FIG. 1. The field-cooled and zero-field-cooled temperature-dependent magnetizations $[M(T)]$ measured at 0.1 T and 0.01 T for (a) the as-deposited (AD) and (b) the oxygen-annealed (PA) films. (c) Similar $M(T)$ measurement for the argon-annealed (ArPA) film at 0.1 T. The typical spin-glass behavior is observed in all films, indicating either the structure disorder or the magnetic disorder is ubiquitously existent in this manganite. The zero-field temperature dependence of resistivity for both films is also displayed. Notice the drastic difference exhibited.

III. RESULTS AND DISCUSSION

A. Transport and magnetic behaviors

Figure 1 shows the field-cooled and zero-field-cooled temperature-dependent magnetizations $M(T)$ measured at applied field of 0.1 T and 0.01 T together with the zero-field temperature dependence of resistivity $\rho(T)$ for (a) the as-deposited (AD) and (b) the oxygen-annealed (PA) LSnMO

films as well as for (c) the argon-annealed (ArPA) LSnMO film measured at 0.1 T, respectively. We note that in the paramagnetic (PM) state the resistivity of the AD film is larger than that of the PA films by nearly two orders of magnitude. While this may originate from the charge localization effects associated with lattice distortion,[22,23] the absence of a temperature-induced T_{IM} in the AD film can be more subtle and complicated. De Teresa *et al.*[24] argued that it might be related to the absence of long range FM order signified with a manifestation of spin-glasslike behavior at lower temperatures. This would imply that the large epitaxial strain originally existent in the AD film not only induces enormous charge localization effect but also hinders the formation of long range FM ordering. If this argument is true, one expects to see the opposites for the PA films. At first glance, it seems to explain the over 200% enhancement in magnetization and dramatic increase in T_{IM} rather consistently. However, as shown in Fig. 1, significant spin-glasslike behavior, characterized by the pronounced irreversibility between the field-cooled (FC) and zero-field-cooled (ZFC) $M(T)$ curves, is evident for both cases. This implies that the insulator-metal transition and spin-glass state are not necessary mutually exclusive. Furthermore, we note that the results shown in Fig. 1 also reveal some features deviating from that reported for low-doping LSnMO.[18] In that progressive suppression of spin-glasslike behavior with increasing Sn doping was observed. It has been interpreted as a result of increasing Mn^{4+} ions driven by Sn doping-induced La vacancies, and the low-doping LSnMO's were essentially regarded as hole-doped manganites. However, according to the XAS results to be presented below, the features of Mn^{2+}/Mn^{3+} mixed valences indicate that the present AD films might have effectively doped some electrons to the e_g band of Mn-3*d* orbitals. Furthermore, we note that, in our case (x=0.3) the spin-glasslike transition not only emerges at much higher temperature ($T_g \approx 150$ K) than that reported in Ref. 14 (75 K→20 K for x =0.04→0.18) but also is very sensitive to the applied field. Thus, we suspect that the Sn-doping-induced La-vacancies scenario may not apply to our case. The spin-glasslike behavior and CMR effect observed in the annealed LSnMO here is probably not arising from the divalent doping-enhanced ferromagnetic interaction and magnetic homogeneity but maybe related to the strain relaxation in a subtler manner. The other feature to be noted is the dramatic suppression of the low temperature magnetization for the AD film when measured at 0.01 T. Since the basic ingredients for spin glass to occur are disorder as well as the magnetic interaction randomness, anisotropy and frustrations,[19] we believe that these factors also account for the dramatic suppression of magnetization in the lower measuring fields for the AD films. Finally, we note that very recent observations by Valencia *et al.*[25] have indicated that, in $La_{2/3}Ca_{1/3}MnO_3$ films, the formation of Mn^{2+} ions due to the instability of Mn^{3+} subjected to prolonged air exposure might also lead to charge localization and, hence, the increasing resistivity and reducing magnetization. However, the relevance of this non-ferromagnetic order originated from divalent Mn component to the observed spin-glasslike behaviors discussed above remains to be clarified.

On the other hand, since post annealing by argon is a common practice for preparing the tetravalent-doped CMR materials, it is important to clarify the effect of argon annealing on LSnMO films. The idea behind this practice was that the excessive oxygen may induce hole doping, and thus, may counteract the expected effect of electron-doped CMR materials. Therefore, annealing in the argon environment may avoid the introduction of holes induced by excess oxygen and could turn out to be a practical method of fabricating electron-doped CMR materials. As illustrated in Fig. 1(c), the M-T of the argon-annealed LSnMO (ArPA LSnMO) film does display a comparable magnetization to that of the PA-LSnMO film. Nonetheless, the zero-field temperature dependent resistivity, $\rho(T)$, is about three times larger than that of the PA-LSnMO film. Since, in contrast to the AD films, both PA- and ArPA-LSnMO films exhibit signatures of typical paramagnetic-insulator (PI) to ferromagnetic-metal (FM) transition, annealing appears to have effects on driving the material from a ferromagnetic insulator to a ferromagnetic metal. However, there exist some differences in the detailed behaviors between the PA and ArPA films, as well.

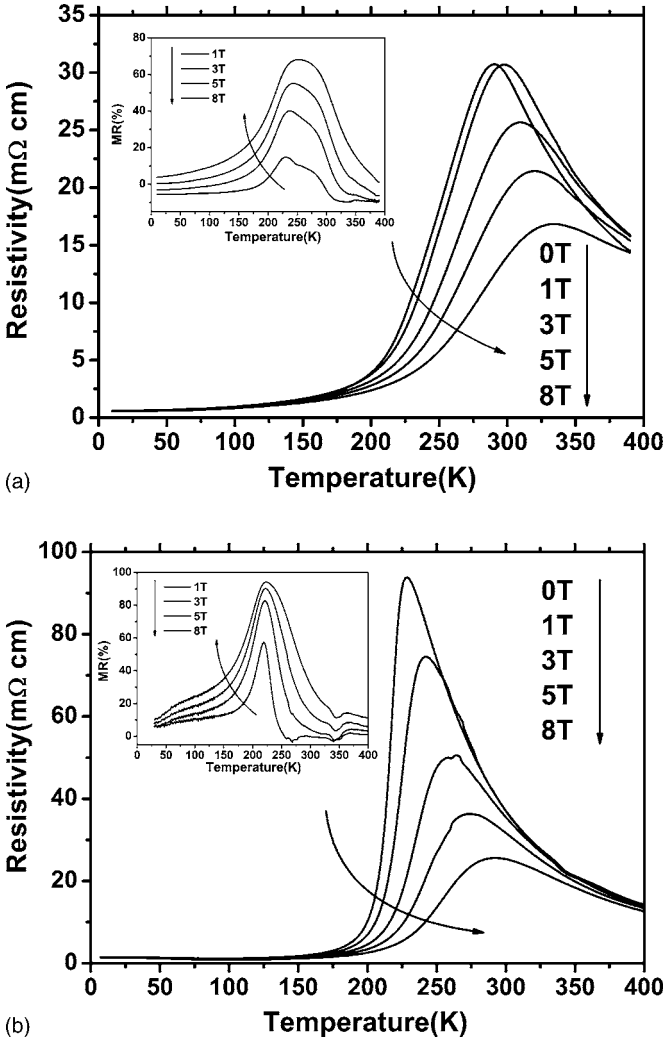

FIG. 2. $\rho(T)$ as a function of applied field for the (a) PA and (b) ArPA LSnMO film, respectively. The inset illustrates the field dependence of the MR ratio.

Figure 2 shows $\rho(T)$ as a function of applied field for the PA film and ArPA film, respectively. The resistivity was mea-

sured with the field applied parallel to the film surface. For the AD film, although there exists a typical PM-FM transition with $T_c \approx 190$ K, the $\rho(T)$ increases steeply with decreasing temperature [Fig. 1(a)] and has no sign of metallic transition for applied field up to 8 Tesla. On the contrary, for the PA film, in addition to having nearly two orders of magnitude reduction in resistivity as compared to the AD film in the PM state, it also displays the typical CMR behavior with $T_{IM} \sim 300$ K at zero field. The maximum magnetoresistance (MR) ratio, defined as $\Delta\rho/\rho=[\rho(0)-\rho(H)]/\rho(0)$ with $\rho(0)$ and $\rho(H)$ being the resistivity at zero field and at field H, appears around 250 K and reaches about 70% at a field of 8 Tesla. Together with the $M(T)$ results shown in Fig. 1, the results demonstrate that annealing not only significantly enhances the low-temperature magnetization by more than 200% but also changes the magnetotransport properties of the LSnMO films dramatically. Guo *et al.*,[17] by varying the film thickness in their $La_{0.9}Sn_{0.1}MnO_{3+\delta}$ films, have found similar enhancement in raising T_{IM} with increasing film thickness. However, there was no noticeable change in T_c and low temperature magnetization with film thickness variations, which led them to conclude that the enhancement of T_{IM} was due to strain relaxation instead of formation of new phases introduced by oxygen or La deficiency.[7,8,20,25–28] Similarly, Thomas *et al.*[29] have attributed the improved magnetotransport properties observed in their high temperature (900 °C) annealed $La_{0.7}Ca_{0.3}MnO_3$ films to the massive stress relaxation and improved film crystallinity accompanied with grain growth. However, they did not report how magnetization and T_c were affected by post annealing. In comparison, for the ArPA films, although it also displays the typical CMR behavior, the $T_{IM}=230$ K at zero field is somewhat lower than that of the PA films. The maximum MR ratio appears around 220 K and reaches nearly about 95% at a field of 8 Tesla. These results are, in fact, very similar to that of some La-deficient CMR materials.[20,24] It appears that, from the magnetotransport properties alone, one cannot discern whether the typical CMR behaviors displayed by post-annealed films are indeed the genuine characteristics of electron-doped manganites or they are just manifestations of La-deficient manganites induced by post annealing.[11] In addition, whether the lack of insulating-metallic transition in AD-LSnMO films is correlated to the lattice disorder or to other mechanisms (such as composition change) remains to be clarified. In order to give some further accounts on these issues, we performed further investigations on the electronic structures of the corresponding films by XAS measurements.

B. Electronic structure

Figure 3(a) shows the XAS results of Mn-$L_{2,3}$ for the AD-, PA-, and ArPA-films together with that of several "standard" powder samples. The results demonstrate that, while the AD-film indeed displays qualitative mixed-valence state characteristics of Mn^{2+}/Mn^{3+}, the valence state of Mn in the PA- and ArPA-films appears to be closer to that of the Mn^{3+}/Mn^{4+} mixed state. The manifestation of Mn^{2+} characteristic revealed in the XAS of the AD-film indicates that the PLD process, though may simultaneously introduce significant structural disorders, does help in retaining the Sn ions in the lattice. On the other hand, both the PA and ArPA processes appear to drive the LSnMO toward the hole-doped regime, except that there is signature of Mn^{2+} (the pre-edge peak around 640 eV) appearing for the latter. In order to further delineate the possible difference between the electronic structure of PA and ArPA films implied in the magne-

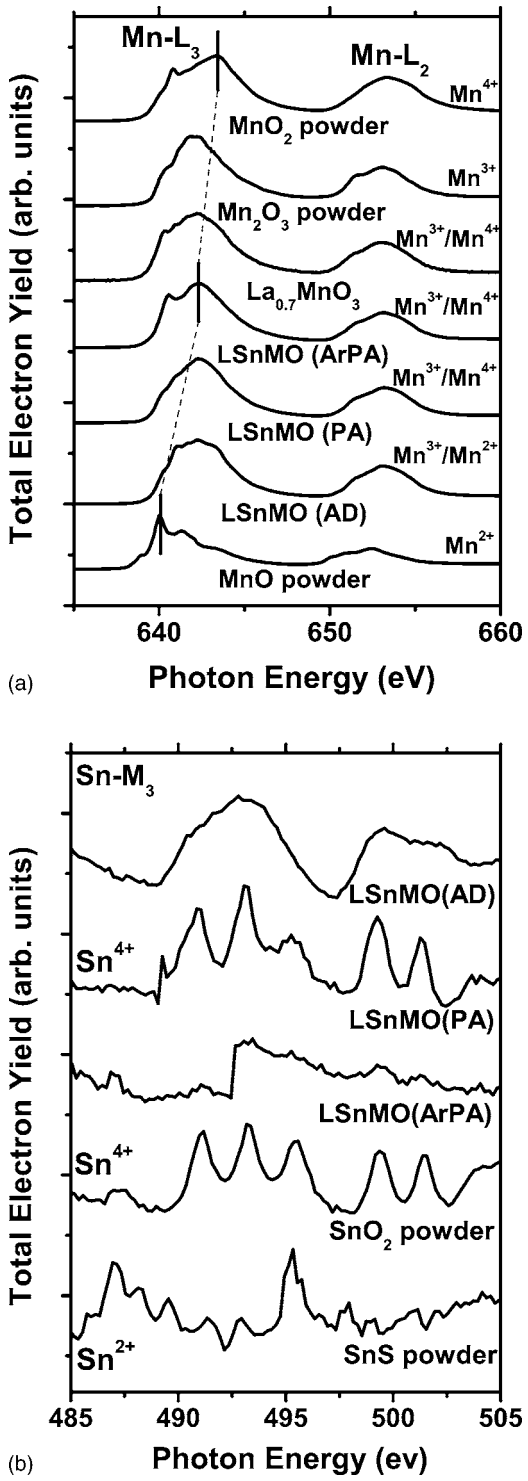

FIG. 3. The x-ray absorption spectra of (a) Mn-$L_{2,3}$ and (b) Sn-M_3 for LSnMO film, respectively. Spectra for various standard reference compounds are also displayed for comparison.

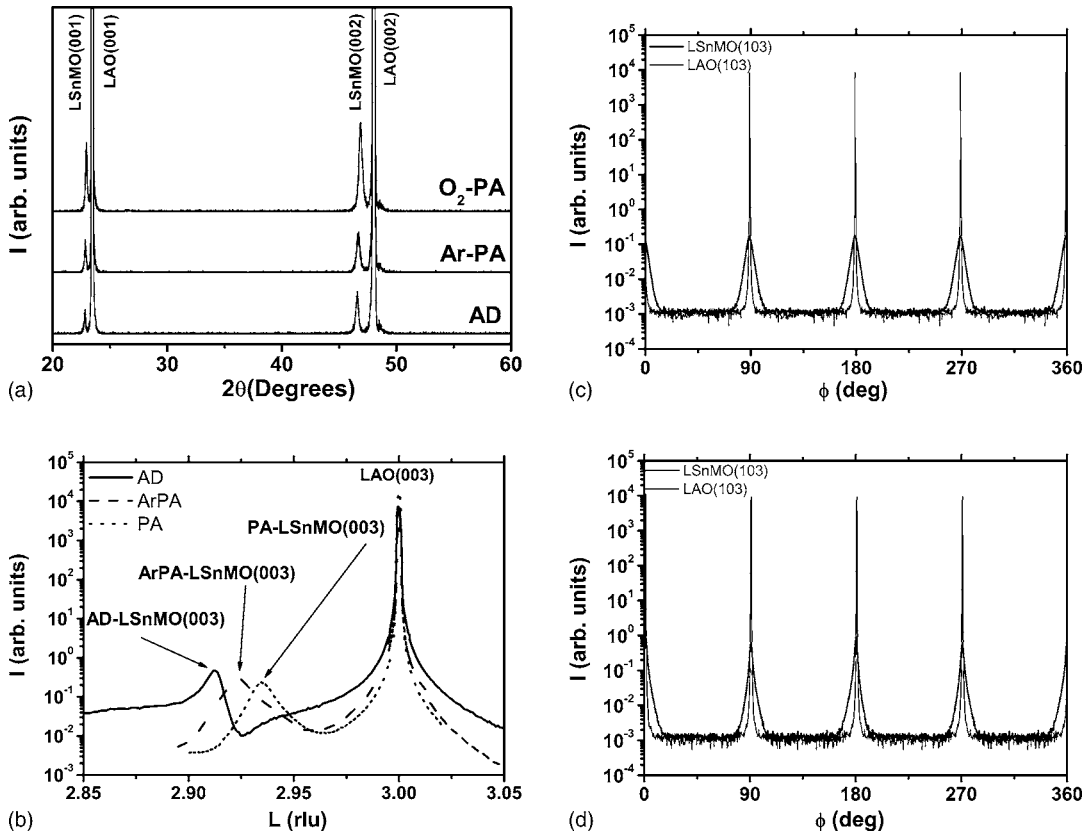

FIG. 4. (a) XRD results for the as-deposited, Ar-annealed and post-annealed LSnMO films grown on LAO substrates at T_s=780 °C. (b) L scan of AD, ArPA, and PA films across (003) Bragg peak. (c) The ϕ scans for the LAO (103) and AD LSnMO (103) Bragg peaks, respectively. (d) The ϕ scans for the LAO (103) and PA LSnMO (103) Bragg peaks, respectively. The results clearly show the high degree of epitaxy between the film and substrate. Significant strain resulted from this kind of coherency is expected.

totransport results described above, we show, in Fig. 3(b), the XAS of Sn together with that obtained from the standard samples of SnO_2 and SnS powder. We first note that the results essentially dismiss the existence of Sn^{2+} ions in the LSnMO films, despite it has been anticipated that the ionic size of Sn^{2+} (0.96 Å) seems to be more favorable than that of Sn^{4+} (0.81 Å) in substituting the La^{3+} (1.13 Å) ions in the perovkite structure.[30] The XAS data of Sn in the PA-LSnMO (oxygen annealed) films qualitatively demonstrate the features obtained from the standard SnO_2 samples, indicating that the majority of Sn ions are in the valence state of Sn^{4+}. In comparison, the XAS of Sn in the AD film displays a smeared characteristic of Sn^{4+} around the same energy range. This is indicative that the Sn ions are residing on the La-site and are either affected by the size-mismatch-induced strain or even participating the hybridization between Mn-3d and O-2p orbitals, as in this case most of Sn ions are retained in the La-Sn-Mn-O films (*vide infra*). On the contrary, the XAS data of Sn in the Ar-annealed film do not show the signature of either Sn^{2+} or Sn^{4+}, suggesting that the doped Sn in the initial target material may have been largely missing in the ArPA LSnMO film, at least within the depth probed by the XAS. We, thus, suspect that the magnetotransport properties demonstrated previously might be the manifestations of some La-deficient manganite derived from the argon-annealed process. Besides, the unambiguous Sn^{4+} feature observed in the PA-LSnMO films suggests that either the valence of Sn in LSnMO is really 4+ or there is some SnO_2 or other tin compounds formed in the LSnMO sample during the oxygen annealing process. Although the high T_c and high T_{IM} exhibited by these films have indicated that the latter is more likely the case, direct evidence is desirable to clarify this issue.

C. Microstructure and constituents distribution analysis

Figure 4(a) compares the θ–2θ scan of x-ray diffraction (XRD) results for AD, ArPA, and PA LSnMO films. As is evident from the results, all the films are c-axis oriented with no observable impurity phases. The slight split of the (00ℓ) peaks between the ArPA and PA films and the substrates, however, indicates that significant strain relaxation may have occurred after prolonged annealing. To further delineate the possible subtle changes in the film microstructure due to annealing, L-scan and ϕ-scan measurements were performed. The typical results are illustrated in Figs. 4(b)–4(d), respectively. In Fig. 4(b), it is evident that, in addition to the sharp Bragg peak from the LAO substrate, well-resolved (003)-reflection peaks of the LSnMO films were observed for the AD, ArPA, and PA samples with the correspondent c-axis lattice constant being 3.908 Å, 3.893 Å, and 3.878 Å, respectively. Since the LSnMO film on LAO substrate is expected to experience an in-plane compressive stress due to the smaller substrate lattice constants, the progressive short-

ening of the *c*-axis lattice constant exhibited in the ArPA and PA films is indicative of the occurrence of annealing-induced strain relaxation, which in turn drives the film toward its bulk characteristics. (The pseudocubic lattice parameter of $La_{1-x}MnO_3$ ranges from 0.3866 nm–0.3880 nm for $x=0-0.33$.[25,28]). We note that the in-plane lattice parameters also exhibited noticeable shrinkage upon annealing with $a=3.913$ Å, 3.907 Å, and 3.900 Å for AD, ArPA, and PA films, respectively. Valencia *et al.*[32] pointed out, in their study of LCMO/STO films, that the existence of oxygen vacancies compensates the excessive elastic energy in coherently strained films. Thus, the shrinkage of the unit cell volume may reflect the elimination of oxygen vacancies and associated strain energy. The full width at half maximum (FWHM) of the (0–13) peak of AD-LSnMO is about 4.4°, which is much larger than that of LAO (103) (0.1°). This can be either due to the strain or fine grain size effects. The in-plane grain size estimated from the linewidth of *K* scan across the LSnMO (0 −1 3) reflection is approximately 100 Å. On the other hand, for the PA film, the FWHM of LSnMO (103) is about 1.9°, which, though still much larger than that of LAO (103) (~0.036°), is significantly smaller than that observed in AD film. The in-plane grain size as estimated from the linewidth of the *H* scan across the LSnMO (103) reflection is approximately 135 Å. This difference strongly suggests the crystallinity of LSnMO films was significantly improved upon annealing while the in-plane epitaxial relations remain largely intact. The ϕ scans were taken along the (0 −1 3) Bragg peak of the LAO substrate and LSnMO films. As is evident from Figs. 4(c) and 4(d), both AD- and PA-LSnMO films display well-aligned *ab*-plane epitaxy with the LAO substrate. Again, the FWHM of the diffraction peaks for the AD film is larger than that of the PA film consistent with the arguments aforementioned for the XRD results.

To further delineate the evolving film/substrate relations due to annealing, Fig. 5(a)–5(c) compares the reciprocal space maps of AD-, ArPA- and PA-LSnMO films. The decreasing peak position offset in $q_{\|}$ between LAO and LSnMO in the reciprocal space maps clearly shows the occurrence of strain relaxation effect after the annealing process. It is also evident that the lattice constants of LSnMO are significantly larger than that of LAO, consistent with the above mentioned results. For comparison, we show, in Fig. 5(d), the similar plot obtained for the PA LSnMO/STO (001). Since the lattice constant of LSnMO falls between STO and LAO and is closer to that of STO, LSnMO grown epitaxially on STO and LAO would experience a tensile/compressive average in-plane strain, respectively. In the case of LSnMO/STO, the films are fully coherent to the substrate, as indicated by the nearly perfect alignment between the center of the STO(113) and LSnMO(113) peak contours. Nevertheless, in both bases, we observe shrinkage of both the *c*-axis lattice constant and unit cell volume of LSnMO upon post-annealing; in LSnMO/STO case, *a*-*b* remains invariant but in the case of LSnMO/LAO, *a*-*b* also decreases slightly. It appears that some of the strain, originally compensated by oxygen vacancy incorporation,[32] was released through the reduction of average unit cell volume. Alternatively, it is also possible that the change of average lattice parameters upon PA is coupled with change of composition, or even second-phase segregations. In any case, the lattice constant change associated relaxation of the strain in the films, though might originate from very different mechanisms, do intimately correlate to the enhanced CMR properties in a consistent manner. Unfortunately, the x-ray analyses seemed inadequate to precisely answer the question about the role played by Sn.

In order to further examine the distribution of Sn and the possibly formed Sn-compounds that are not discernable by using x-ray diffraction alone, we performed the cross-sectional transmission electron microscopy (X-TEM) analyses to reveal the microstructure and the element distribution of the LSnMO films. Figures 6(a) and 6(b) Show the bright-field TEM images and selective area diffraction (SAD) pattern of AD LSnMO(001) film grown on LAO(001) substrate. As can be seen from Fig. 6(a), the film microstructure appears to be rather homogeneous and there is no trace of any additional compound existing within the interface of film and substrate. In addition, the absence of extra diffraction spots in Fig. 6(b) indicates that the AD-LSnMO film grown on LAO substrate is indeed single phase with well-organized epitaxial relations. The rodlike diffraction spots and the streaky patterns appeared in the columnar grains of the LSnMO phase suggest that there exists a significant amount of strain in the film. We believe that both the slight lattice mismatch between the film and substrate and the large ionic size difference between La^{3+} and Sn^{4+} may contribute. For the PA-LSnMO film, however, the results are quite different. The bright field image shown in Fig. 6(c) apparently displays two somewhat separated regions. The grains in the near surface upper region appear to be more "equiaxial" with much less strain-induced streaky patterns, suggesting significant recrystallization may have occurred due to annealing. In the "lower" region (region close to the substrate interface) the features are more like that observed in the AD film. Although it is still not obvious to conclude whether or not the recrystallized upper region containing any newly formed phases from the SAD results, it is, nevertheless, interesting to find that the oxygen annealing affects only the upper part of the film. With the about 4 h of annealing time and 100 nm of the affected depth, the estimated oxygen diffusion rate at 800 °C is about 25 nm/hr.

From the above discussion, the strain relaxation effect is consistent with what observed in x-ray diffraction analyses and hence account for part of the magnetotransport properties obtained. The XAS results, however, remain to be clarified. In order to delineate the effect of annealing on the composition distribution of the doped element in the LSnMO film, the electron energy loss spectroscopy (EELS) mapping was performed on the TEM samples. Fig. 7(a) show the zero-loss image of the AD-LSnMO film and the elemental maps of La, Sn, Mn, O, respectively. As revealed by the series of the images, the four constituents distribute uniformly over the entire AD-LSnMO film, indicating that they are presumably situated within the parent perovskite structure. The results are largely consistent with the data discussed above. Nevertheless, the elemental maps of the four constituent elements in the PA-LSnMO film display rather different results. As illustrated in Figs. 7(b) there are clear evidence of local segregation of Sn and O in the "upper" region of the

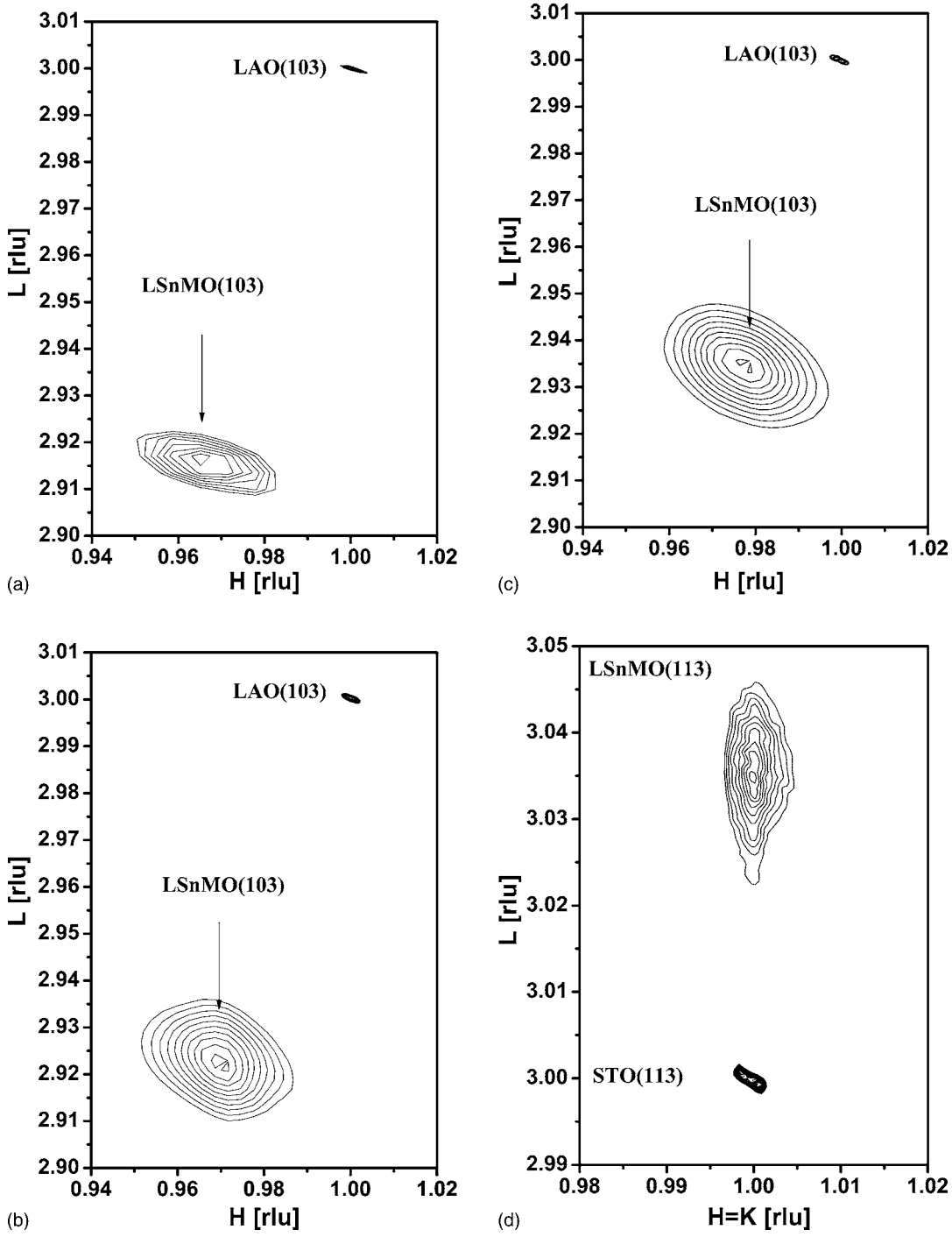

FIG. 5. (a), (b), and (c) are reciprocal space maps of AD, ArPA, and PA LSnMO films grown on LAO substrates, respectively. (d) Reciprocal space map of PA LSnMO film grown on STO substrate.

PA-LSnMO film [Figs. 7(b)]. More interestingly, in these Sn-O segregated areas, both La and Mn are absent [Fig. 7(b)], indicating that the clusters formed are some kind of Sn-O compound. (From the previous XAS results it should be SnO_2.) This strongly implies that the oxygen annealing affected regions may indeed induce the formation of the La-deficient manganite, which, in turn, accounts for the marked enhancement in T_c and T_{IM} for the PA-LSnMO films described above.

In the following, we try to put the experimental observations presented above together to see if it can be reconciled to the outstanding issues about the CMR effects on Sn-doped manganites that we set forth to resolve at the beginning. The very first question to be answered is whether or not Sn ions can substitute La sites? The results obtained from the as-deposited films indicated that the substitution of the tetravalent Sn into the La site does prevail and result in a ferromagnetic-insulating manganite. The unexpected insulat-

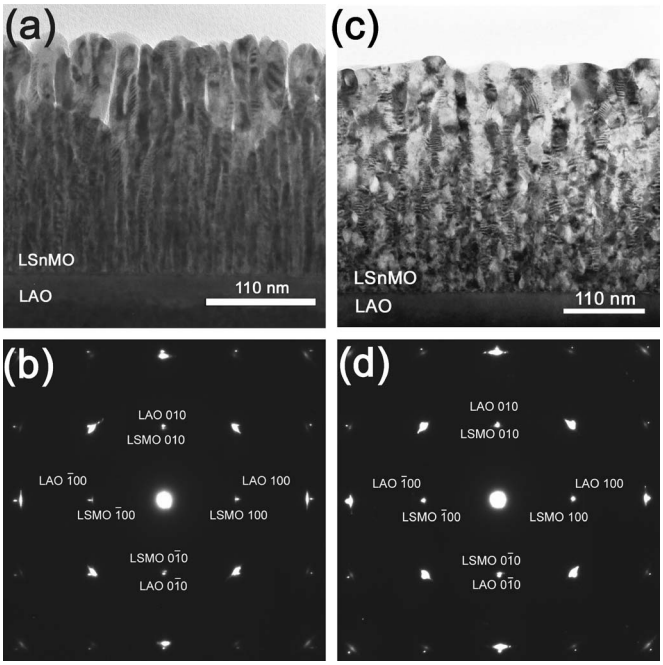

FIG. 6. (a) The bright-field TEM image and (b) the electron diffraction pattern for the AD LSnMO (001) film. (c) The bright-field TEM image and (d) the electron diffraction pattern for the PA LSnMO (001) film. Notice that the near-surface upper part of the PA LSnMO film displays apparent recrystallization signature upon prolonged annealing.

ing behavior thus suggests either the lack of itinerant carriers or a fundamentally different exchange mechanism in the electron-doped regime. In the former scenario, similar double-exchange mechanism as in the hole-doped manganites gives rise to the paramagnetic-ferromagnetic transition and the existence of Mn^{2+} due to tetravalent doping of Sn^{4+} should result in enhancement of saturation magnetization below T_c owing to contributions from extra e_g electrons. However, due to the charge localization effects associated with strain-induced lattice distortion, the lack of itinerant electrons not only has hindered effective transport but also is responsible for the absence of long range FM order as manifested in the dramatic reduction of saturation magnetization and marked spin-glasslike behavior displayed in Fig. 1. The large epitaxial strain originally existent in the AD-film as revealed by the x-ray and X-TEM analyses seemed to give consistent support. On the other hand, the existence of Mn^{2+} in as-deposited and prolonged air exposure LCMO films was found to yield charge localization, and hence increasing resistivity and reducing magnetization, as well.[25] However, the effects of Mn^{2+}-induced charge localization seemed too modest to drive it into ferromagnetic insulator. Another possibility for explaining why our AD LSnMO films present as a ferromagnetic insulator is that the doping level (x=0.3) is too low to drive the LSnMO into n-type manganite. Chang *et al.*[12] indicated that the one of the main effects of doping Ce (up to x=0.3) into $LaMnO_3$ was to dramatically shrink the hole pockets near the Fermi level, instead of providing itinerant electrons and driving LCeMO into a n-type manganite. We believe that, from the evidence exhibited by XAS (espe-

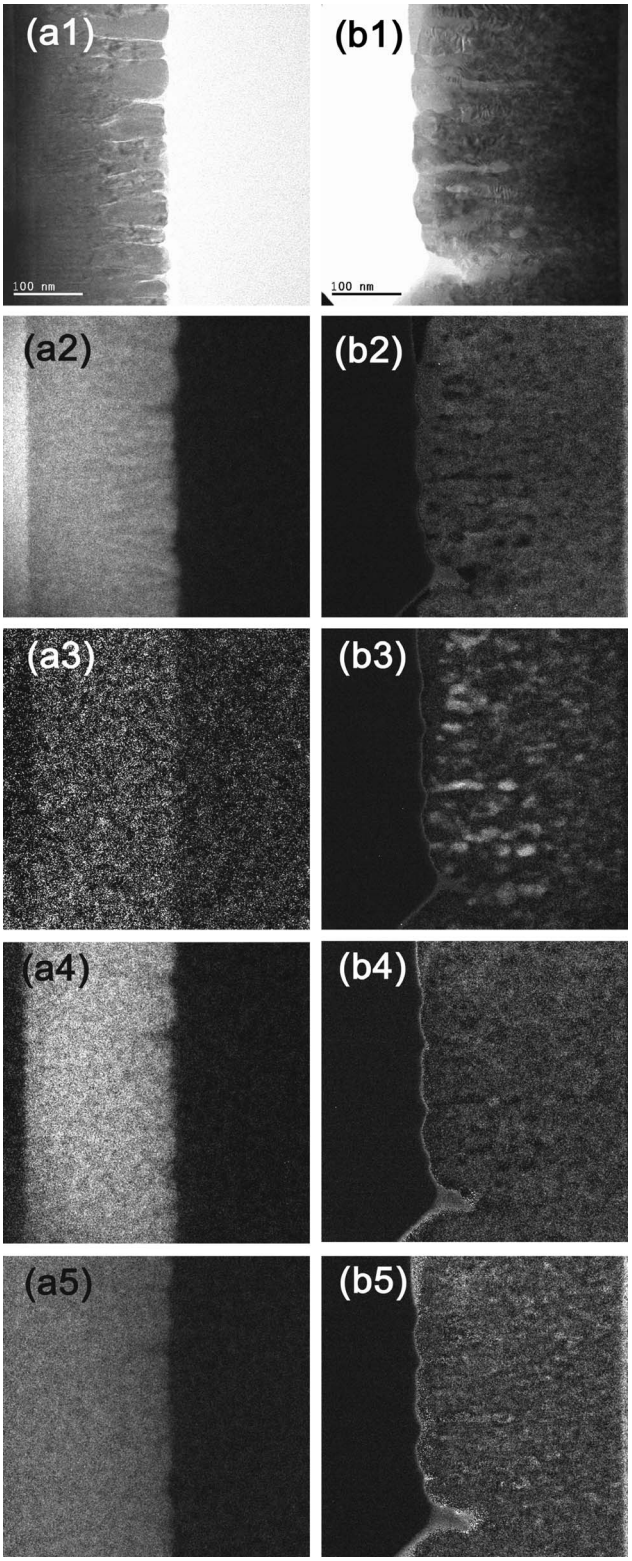

FIG. 7. (a) The electron energy loss spectroscopy of the zero-loss image (a1) and the elemental maps of La (a2), Sn (a3), Mn (a4), and O (a5) of the AD LSnMO film. (b) The electron energy loss spectroscopy of the zero-loss image (b1) and the elemental maps of La (b2), Sn (b3), Mn (b4), and O (b5) of the PA LSnMO film.

cially on Sn ion) and EELS of XTEM analyses, for AD-LSnMO films, effective doping is obtained. However, the tetravalent—doping-induced hole-pocket shrinkage effects similar to that observed in Ce-doped manganites[12] may also happen in the present AD-LSnMO films. Together with the influences of the coherent strain and, possibly larger ion-size effect, thus resulted in the ferromagnetic insulating as well as spin-glasslike behaviors displayed by the AD-LSnMO films.

On the other hand, although post annealing under oxygen or argon is usually practiced in the fabrication of the "electron-doped" manganites, our experimental results demonstrate that it may not work as expected. According the XAS of Sn, we are tempted to rule out the existence of Sn^{2+} ions in the LSnMO films. The XAS of Sn for the PA-LSnMO film evidently shows the characteristics of Sn^{4+} valence. On the contrary, the same spectrum for the Ar-annealed film does not show the characteristics of either Sn^{2+} or Sn^{4+}, suggesting that the doped Sn in the initial target material may have been largely missing in the ArPA-LSnMO film. The question is how do these spectrum results correlated to the magnetotransport properties displayed by the respective films? The TEM microstructure analyses and the EELS elemental map of PA-LSnMO film evidently showed that there is some kind of Sn-O compound formed during the post annealing. The unambiguous Sn^{4+} feature of XAS results strongly implies that within the oxygen annealing affected regions it may have indeed induced the formation of the La-deficient manganite with SnO_2 clusters. The significant improvement of the CMR effects, including high T_c, T_{IM}, low resistivity and relatively large magnetization at low temperatures, is naturally explained within the context of this scenario. Finally, for the ArPA-LSnMO films, although also exhibit transitions from paramagnetic insulator to ferromagnetic metal albeit at a significantly lower temperature with higher resistivity, the detailed mechanism may be fundamentally different from the oxygen-annealed PA-LSnMO films. In particular, the XAS of Sn for this film showed most of the Sn was missing after annealing. Thus, although the reduced average unit-cell volume for the ArPA- and PA-LSnMO films is indicative of strain relaxation, it is doubtful to attribute it as the sole reason for the obtained enhancement on the magnetotransport properties. It is quite possible that the change of average lattice parameters upon annealing is also coupled with change of composition, or even segregation of second phases. In this scenario, the excessive oxygen presumably present in the PA-LSnMO films would provide more itinerant carriers and Mn^{4+} content,[32] and is responsible for the improvement of electrical transport and magnetic properties. While Ar-annealing, though may induce the loss of Sn and hence result in La-deficient manganite, it may also provoke the formation of nonferromagnetic Mn^{2+} component and give rise to charge localization-induced increase in resistivity and reduction in saturated magnetization.[25]

Finally, we make a brief comparison between LSnMO and LCeMO, the two representative "electron-doped" manganites. The primary distinction of these two materials is the ionic size difference of Sn^{4+} (0.81 Å) and Ce^{4+} (0.97 Å).[31] One of the instant effects resulted from this was the low temperature saturation magnetization obtained from the as-deposited films with $M_{LCeMO} \sim 1.4\ \mu_B$/Mn-site[13] and $M_{LSnMO} \sim 0.4\ \mu_B$/Mn-site measured under $T=10$ K, $H=100$ Oe. This may be easily attributed to more severe structure disorder originated from the larger ionic size difference between Sn^{4+} and La^{3+} (0.32 Å) than that between Ce^{4+} and La^{3+} (0.16 Å). However, as the films were annealed under oxygen environment, both LSnMO and LCeMO exhibit similar magnetotransport properties. The existence of SnO_2 or CeO_2 (Ref. 13) seemed to indicate that both films tend to turn into La-deficient manganites after annealing. However, for as-deposited PLD LCeMO films, there are still some discrepancies on the magnetotransport properties reported in the literature remained to be clarified.[9–13]

IV. CONCLUSIONS

In summary, we have presented systematic investigations on one of the highly anticipated electron-doped CMR materials. Single-phase $La_{0.7}Sn_{0.3}MnO_3$ (LSnMO) thin films were grown on $LaAlO_3$ substrates by pulsed laser deposition. The as-deposited LSnMO films are ferromagnetic insulators with typical Curie temperature around 150 K. Both the electronic structure revealed by the x-ray absorption spectra (XAS) and the detailed TEM analyses indicate that in this case the doped Sn-element is indeed acting as the tetravalent ion uniformly distributed in the $LaMnO_3$ parent compound. The large internal strain originated from the marked ion size difference between the doped Sn^{4+} and substituted La^{3+} ions, however, is believed to hinder the long-range itinerancy of the carriers, hence preventing it from becoming metallic. Unfortunately, due to the insulating nature of these as-deposited LSnMO films, it is not clear whether it is indeed "*n*-type" electron-doped manganite. *Ex situ* annealing in oxygen and argon both drive the films to exhibit insulator-metal transition with hole-doped characteristics when becoming ferromagnetic. The transition temperatures, however, are different for films annealed in different environments, presumably due to the final phase and compositions obtained. From the results of magnetoresistance measurements and XAS, it is suggestive that LSnMO films annealed in argon causes the significant loss of Sn and results in La-deficient phase. Whereas those annealed in oxygen appeared to form some kind of Sn-O compound, turning the films into La-deficient manganite, albeit with some excessive oxygen. We emphasize that the existence of tetravalent Sn from x-ray absorption spectroscopy (XAS) should not be taken as the sole evidence of achieving electron-doped manganite. As being clearly demonstrated in this study, it may just reveal the emergence of SnO_2.

ACKNOWLEDGMENTS

This work is supported by the National Science Council of Taiwan, R.O.C. through Grant No.NSC94-2112-M009-007.

*Corresponding author. Email address: melin.ep91g@nctu.edu.tw

[1] Y. Tokura and N. Nagaosa, Science **288**, 462 (2000), and references therein.
[2] E. Dagotto, "*Nanoscale Phase Separation and Colossal Magnetoresistance*" (Springer, 2003), and references therein.
[3] C. Zener, Phys. Rev. **82**, 403 (1951).
[4] A. J. Millis, P. B. Littlewood, and B. I. Shraiman, Phys. Rev. Lett. **74**, 5144 (1995).
[5] V. L. Joseph Joly, P. A. Joy, and S. K. Date, J. Magn. Magn. Mater. **247**, 316 (2002).
[6] S. Das and P. Mandal, Z. Phys. B: Condens. Matter **104**, 7 (1997); P. Mandal and S. Das, Phys. Rev. B **56**, 15073 (1997).
[7] A. Gupta, T. R. McGuire, P. R. Duncombe, M. Rupp, J. Z. Sun, W. J. Gallagher, and Gang Xiao, Appl. Phys. Lett. **67**, 3494 (1995).
[8] S. Pingard, H. Vincent, J. P. Senateur, J. Pierre, and A. Abrutis, J. Appl. Phys. **82**, 4445 (1997).
[9] C. Mitra, P. Raychaudhuri, J. John, S. K. Dhar, A. K. Nigam, and R. Pinto, J. Appl. Phys. **89**, 524 (2001).
[10] W. J. Chang, C. C. Hsieh, J. Y. Juang, K. H. Wu, T. M. Uen, Y. S. Gou, C. H. Hsu, and J.-Y. Lin, J. Appl. Phys. **96**, 4357 (2004).
[11] T. Yanagida, T. Kanki, B. Vilquin, H. Tanaka, and T. Kawai, Solid State Commun. **129**, 785 (2004).
[12] W. J. Chang, J. Y. Tsai, H.-T. Jeng, J.-Y. Lin, Kenneth Y.-J. Zhang, H. L. Liu, J. M. Lee, J. M. Chen, K. H. Wu, T. M. Uen, Y. S. Gou, and J. Y. Juang, Phys. Rev. B **72**, 132410 (2005).
[13] Takeshi Yanagida, Teruo Kanki, Bertrand Vilquin, Hidekazu Tanaka, and Tomoji Kawai, Phys. Rev. B **70**, 184437 (2004).
[14] Guotai Tan, X. Zhang, and Zhenghao Chen, J. Appl. Phys. **95**, 6322 (2004).
[15] Ping Duan, Zhenghao Chen, Shouyu Dai, Yueliang Zhou, Huibin Lu, Kuijuan Jin, and Bolin Cheng, Appl. Phys. Lett. **84**, 4741 (2004).
[16] J. Gao, S. Y. Dai, and T. K. Li, Phys. Rev. B **67**, 153403 (2003).
[17] X. Guo, S. Dai, Y. Zhou, G. Yang, and Z. Chen, Appl. Phys. Lett. **75**, 3378 (1999).
[18] X. Guo, Z. Chen, S. Dai, Y. Zhou, R. Li, H. Zhang, B. Shen, and H. Cheng, J. Appl. Phys. **88**, 4758 (2000).
[19] J. A. Mydosh, *Spin Galsses: An Experimental Introduction* (Taylor & Francis, London, 1993).
[20] S. de Brion, F. Ciorcas, G. Chouteau, P. Lejay, P. Radaelli, and C. Chaillout, Phys. Rev. B **59**, 1304 (1999).
[21] T. Y. Cheng, C. C. Hsieh, J. Y. Juang, J.-Y. Lin, K. H. Wu, T. M. Uen, Y. S. Gou, and C. H. Hsu, Physica B **365**, 141 (2005).
[22] M. R. Ibarra, P. A. Algarabel, C. Marquina, J. Blasco, and J. García, Phys. Rev. Lett. **75**, 3541 (1995).
[23] P. G. Radaelli, D. E. Cox, M. Marezio, S.-W. Cheong, P. E. Schiffer, and A. P. Ramirez, Phys. Rev. Lett. **75**, 4488 (1995).
[24] J. M. De Teresa, M. R. Ibarra, J. García, J. Blasco, C. Ritter, P. A. Algarabel, C. Marquina, and A. del Moral, Phys. Rev. Lett. **76**, 3392 (1996).
[25] S. Valencia, A. Gaupp, W. Gudat, Ll. Abad, Ll. Balcells, A. Cavallaro, B. Martínez, and F. J. Palomares, Phys. Rev. B **73**, 104402 (2006).
[26] S. J. Kim, C. S. Kim, S. I. Park, and B. W. Lee, J. Appl. Phys. **89**, 7416 (2001).
[27] B. C. Hauback, H. Fjellvag, and N. Sakai, J. Solid State Chem. **124**, 43 (1996).
[28] G. J. Chen, Y. H. Chang, and H. W. Hsu, J. Magn. Magn. Mater. **219**, 317 (2000).
[29] R. Suryanarayanan, J. Berthon, I. Zelenay, B. Martínez, X. Obradors, S. Uma, and E. Gemelin, J. Appl. Phys. **83**, 5264 (1998).
[30] K. A. Thomas, P. S. I. P. N. de Silva, L. F. Cohen, A. Hossain, M. Rajeswari, T. Venkateson, R. Hiskes, and J. L. MacManus-Driscoll, J. Appl. Phys. **84**, 3939 (1998).
[31] R. D. Shannon, Acta Crystallogr. **32**, 752 (1976).
[32] S. Valencia, Ll. Balcells, J. Fontcuberta, and B. Martínez, Appl. Phys. Lett. **82**, 4531 (2003).